EFFECT OF SOURCE X-RAY ENERGY SPECTRA ON THE DETECTION OF FLUORESCENCE PHOTONS FROM GOLD NANOPARTICLES

A Thesis
Presented to
The Academic Faculty

by

Nivedh H. Manohar

In Partial Fulfillment
of the Requirements for the Degree
Master of Science in Medical Physics in the
George W. Woodruff School of Mechanical Engineering

Georgia Institute of Technology
December 2011

EFFECT OF SOURCE X-RAY ENERGY SPECTRA ON THE DETECTION OF FLUORESCENCE PHOTONS FROM GOLD NANOPARTICLES

Approved by:

Dr. Sang Hyun Cho, Advisor
School of Mechanical Engineering
Georgia Institute of Technology

Dr. C.-K. Chris Wang
School of Mechanical Engineering
Georgia Institute of Technology

Dr. Eric Elder
Department of Radiation Oncology
Emory University School of Medicine

Date Approved: November 11, 2011

ACKNOWLEDGEMENTS

First and foremost, I would like to thank my advisor and mentor Dr. Sang Hyun Cho for sharing his immense knowledge with me, providing persistent support, and offering unfailing encouragement. Also, I am very grateful for the current and former members of our research group for paving the way in making this work possible: Dr. Seong-Kyun Cheong, Dr. Bernard "Tripp" Jones, Fang Liu, Arsalan Siddiqi, and others. I would also like to thank my thesis committee members Dr. C.-K. Chris Wang and Dr. Eric Elder for all of their help and support.

TABLE OF CONTENTS

LIST OF TABLES

LIST OF FIGURES

SUMMARY

The purpose of this work was to assess the effect of x-ray source spectra on the detection of fluorescence photons from gold nanoparticles (GNPs) in the context of a bench-top x-ray fluorescence computed tomography (XFCT) system.

A computational Monte Carlo (MC) model of the pre-existing experimental XFCT system was created using the Monte Carlo N-Particle (MCNP) code system. The model was used to simulate irradiation of a small animal-sized plastic phantom containing GNP-loaded water columns with a Pb filtered polychromatic x-ray source. Simulations were run to verify the validity of the MCNP model as an accurate representation of the actual system by means of comparison with experimentally-obtained data. Once verified, the model was used for further purely computational work.

Subsequently, MC simulations were repeated with the source replaced by hypothetical monochromatic and quasi-monochromatic x-ray sources (81, 85, 90, 95, and 100 keV) to determine the most ideal source x-ray energy in order to discriminate between gold *K*-shell fluorescence peaks and the Compton scatter background. As a practical alternative to monochromatic x-rays, a quasi-monochromatic x-ray spectrum experimentally generated from the polychromatic x-ray spectrum of the 105 kVp beam by using a highly oriented pyrolitic graphite (HOPG) crystal was then used in the simulations. This spectrum was used for further MC simulations to assess the effect of a quasi-monochromatic x-ray spectrum on the detection of gold *K*-shell fluorescence x-rays.

Noting the difficulty of using HOPG, conventional filtration methods were explored. The MCNP code was employed to simulate the filtration of the original polychromatic x-ray source by a Thoraeus-type filter. Experiments were also performed to achieve similar filtration using combinations of Sn, Cu, and Al.

It was found that quasi-monochromatic x-ray energy needed to exceed approximately 95 keV in order for the gold *K*-alpha fluorescence peaks (67 and 69 keV) to be easily discernible over the Compton scatter background. At the same GNP concentration, there was at least a three-fold increase in the gold fluorescence signal-to-background ratio from using the HOPG-generated quasi-monochromatic source spectrum, compared to that from using the Pb filtered polychromatic source spectrum.

The effect of these changes on gold fluorescence production was documented and quantified using the signal-to-background ratio and other qualitative measures. The results from this work provided clues on how to improve the detection of gold fluorescence photons from GNP-loaded objects using the XFCT system. This will benefit future research on the development of the XFCT system in the context of making it more feasible for GNP-based preclinical molecular imaging applications.

Since a monochromatic synchrotron x-ray beam, although ideal, is not readily available for a bench-top XFCT system, quasi-monochromatization of a polychromatic x-ray source spectrum to peak at certain energies appeared to help dramatically improve the detection efficiency of *K*-shell fluorescence x-rays from GNPs.

CHAPTER 1

INTRODUCTION

X-ray fluorescence is a well-understood phenomenon in which irradiation of certain atoms with relatively high-energy x-rays causes the emission of characteristic "secondary" x-rays of lower energy. Though there are already several established uses of x-ray fluorescence, our research group aims to utilize this phenomenon for a novel application in nanoparticle-aided cancer imaging and therapy involving the use of gold nanoparticles (GNPs) [1-2]. Gold atoms, when irradiated with x-rays above particular threshold energies, emit characteristic fluorescence x-rays with energies of approximately 10, 67, 69, and 79 keV. These fluorescence peaks can be detected by means of spectroscopy and, with an appropriate experimental setup enabling computed tomography, the GNPs can be imaged inside an object. In effect, the locations of the GNPs can be determined with precision and even the concentration of the GNPs can be inferred based on the strength of the detected fluorescence signal [3].

In vivo, due to the enhanced permeability and retention effect, unconjugated GNPs can be slightly tumor-specific; this phenomenon can be greatly magnified if the GNPs are conjugated with tumor-specific markers. Therefore, the ability to accurately image them has great implications in not only tumor detection but also in new frontiers of research involving cancer treatment modalities using GNPs as tumor-specific "radiosensitizers" or "radiation dose enhancers" such as in so-called "gold nanoparticle-aided radiation therapy (GNRT)" [2, 4-8].

Our research group has already established the basic proof-of-principles for a bench-top x-ray fluorescence computed tomography (XFCT) system that can be used to image GNPs inside small animal-sized objects using both pencil-beam and cone-beam sources [9-10]. Although there are several obstacles, the ultimate goal is to build a practical bench-top XFCT system that can be used for routine *in vivo* molecular imaging with GNPs.

CHAPTER 2

BACKGROUND

2.1 Experimental XFCT System

This work was based on the cone-beam implementation of the XFCT system that consists of several components [7, 10]. These include (1) a Hamamatsu microfocus x-ray source, operating at 105 kVp and a tube current of 400-455 μA, (2) a beam collimator made of lead (Pb), (3) a Pb filter to modify the source x-ray spectrum, (4) a phantom to represent a test specimen, made of polymethyl methacrylate (PMMA), with three slots for inserts, (5) three small tubes, containing solutions of GNPs in water at various concentrations, which can be inserted into the phantom, (6) a shielded and collimated Amptek XR-100T CdTe-based x-ray detector to detect the fluorescence and scattered x-rays from the phantom.

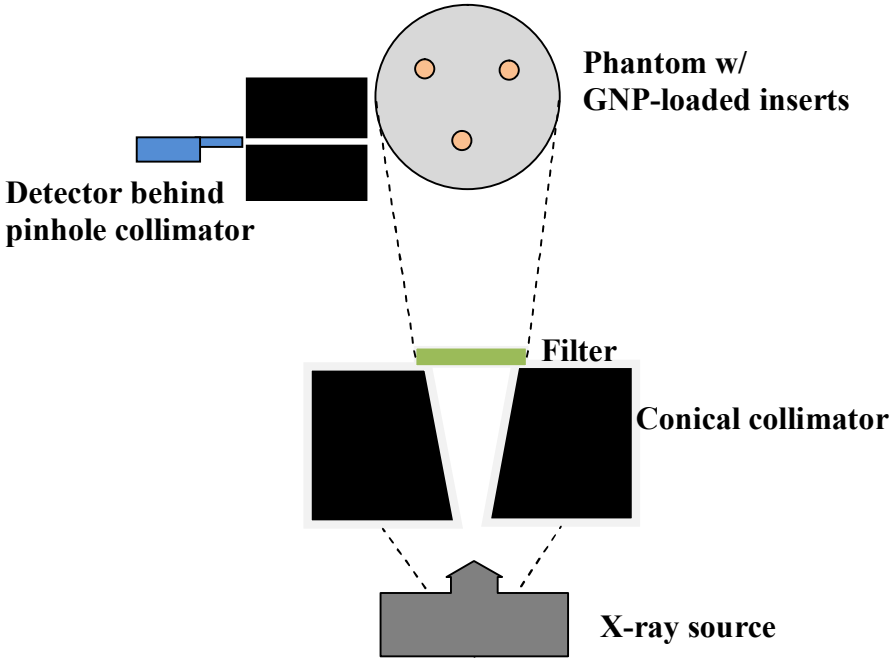

Figure 2.1: Experimental setup of XFCT system

2.2 Importance of X-ray Source Energy Spectrum

Conventional XFCT techniques use monochromatic x-rays, normally produced by a synchrotron [11]. For a bench-top XFCT system usable for *in vivo* imaging, the luxury of a synchrotron is definitely not an option due mainly to space and expense considerations. However, an ordinary diagnostic energy x-ray source producing polychromatic x-rays is readily available.

Our research group has already demonstrated that XFCT imaging using a typical 110 kVp microfocus x-ray source is feasible for a small animal-sized object containing water-filled tubes loaded with GNPs at low concentration. Due to the physics of the photoelectric effect, photon energy must exceed 80.7 keV for *K*-shell fluorescence to occur in gold; therefore, one of the issues that must be addressed before the XFCT system can be made practical is the optimization of the x-ray source spectrum [9]. An optimized x-ray source spectrum, in the context of quasi-monochromatization, would not only help lower the current detection limit for GNPs, but it would also decrease scanning time and reduce unnecessary dose from low energy photons which do not contribute to fluorescence production anyway [12-13].

2.3 Utility of Monte Carlo Methods

Considering the novel nature of the XFCT system, it is unknown what the optimal source spectrum is. The fact that x-ray fluorescence is a relatively inefficient physical process, compounded by issues such as attenuation and interference from the primary x-ray beam, makes accurate detection of fluorescence peaks a challenge. Since the experimental work was believed to have been done at an ideal geometry [14], optimizing

the x-ray source spectrum would be the next logical step to increase the efficiency of fluorescence production and detection.

Although such an optimization could be done experimentally, it can be very time-consuming and expensive to do an exhaustive analysis. Meanwhile, computational approaches based on the Monte Carlo (MC) method have been proven to have great utility in such cases. MC methods are characterized by their use of algorithms that rely on random sampling to compute results. The essence of Monte Carlo is the application of probability and statistics to solve deterministic problems. In essence, individual probabilistic events are simulated to obtain a "big picture" type of solution. The MC method is often used to predict the results from inherently stochastic processes, such as radiation transport.

A fully integrated software package known as the Monte Carlo N-Particle (MCNP) Code, developed by Los Alamos National Laboratory, is one of the industry standard tools used for radiation transport and was chosen as the tool of choice for this work [15]. Being a general-purpose code, it can be used to simulate the transport of various particles through matter. MCNP includes vast libraries of data, such as cross section tables for many materials, making it well-suited for radiation transport. It is capable of "detailed history" computations for uncharged particles such as photons wherein every interaction is simulated. For charged particles such as electrons, it uses a less accurate "condensed history" approach that models step-by-step discrete energy losses, as opposed to individual interactions. For this work, since only photons were of interest, MCNP was extremely well-suited.

CHAPTER 3

METHODOLOGY

The methodology used in this work consisted of three distinct steps: modeling, verification, and investigation. First, a computational model was created using the MCNP code based on the experimental setup of the existing XFCT system. Next, simulations were run to verify the validity of the MCNP model as an accurate representation of the actual system by means of comparison with experimentally-obtained data. Finally, the model was used for further purely computational work investigating the effect of x-ray energy spectra on gold fluorescence detection.

3.1 Monte Carlo Modeling of Experimental Setup

Each component of the XFCT system was modeled accurately in MCNP without extraneous details which could increase computational overheads without providing any benefit in terms of validity of the simulations.

3.1.1 X-ray Source

The x-ray source modeling was based on the Hamamatsu L9631 microfocus x-ray source, which had a maximum output of 110 kVp at 800 μA (run at 105 kVp and 455 μA for experiments). The maximum x-ray emission angle was 62º and the minimum focal spot size was 15 μm. The beam exited through a circular window made of beryllium. Using radiographic film, the geometric properties of the beam were measured to be used for modeling. It was modeled as a biased disk source with a diameter of 1.5 mm, emitting

photons with appropriate angular divergence. The typical source energy spectrum is shown in Fig. 3.1.

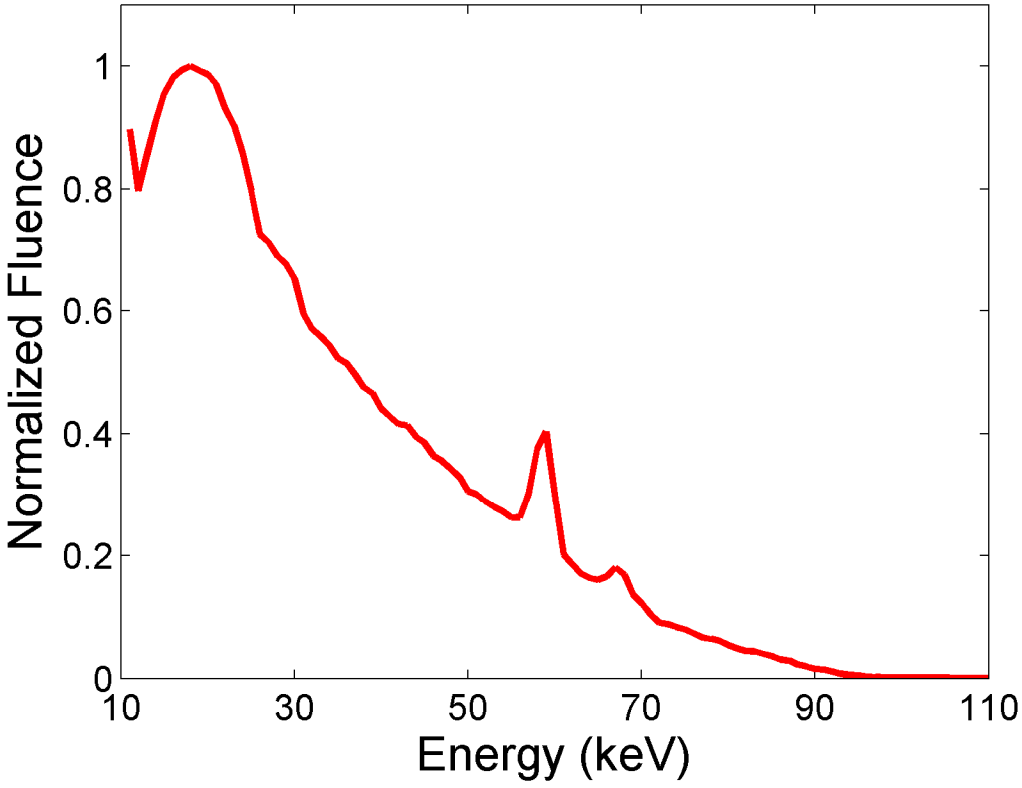

Figure 3.1: Typical x-ray source spectrum

3.1.2 Source Collimator and Filter

The photons emitted from the source eventually reached a lead block, located 16.5 mm away from the source. The block had lateral dimensions of 20 cm in each direction and a thickness in the beam direction of 5 cm. The beam was collimated by a conical hole (11.4º) with diameters of 1 cm and 2 cm in the beam direction. This simple collimator was modeled accurately using MCNP macrobodies. The divergence of the beam after the collimator allowed it to cover the entire phantom, described below.

At the exit of the collimator, a thin lead filter with a thickness of 1 mm was placed in order to attenuate some of the low-energy photons below the gold *K*-edge. Since these low-energy photons do not result in the production of characteristic *K*-shell x-rays from gold anyway, their suppression should increase the signal-to-background ratio for the peaks of interest. However, this beam hardening would also result lower overall photon fluence. This filter was modeled as a simple, homogeneous object of constant thickness.

3.1.3 Phantom and Inserts

With respect to the filter, a cylindrical PMMA phantom was modeled 8 cm away. It had an effective height and diameter of 30 mm, which sat on top of a PMMA base with height of 20 mm and diameter of 45 mm. There were three equally spaced holes drilled at the top with centers at 10 mm from the center of the phantom, diameter of 6 mm and depth 15 mm. Containers of slightly smaller height and diameter were placed in these holes. Two plugs were filled with water, while the third plug was filled with a solution of 2 wt. % GNPs.

3.1.4 Detector and Collimator

The detector was based on the Amptek XR-100T [16] gamma and x-ray detector. It was placed at 90° with respect to the beam direction and 0.75 cm behind a 4-cm-thick Pb pinhole collimator with aperture diameter of 2.5 mm.

The detector points at approximately the center of the plug containing GNPs. The other holes were plugged with PMMA plugs. This makes the simulation, in effect, a snapshot of one of the detector positions and phantom angle during a full computed tomography scan.

The predominant element of the detector is its hermetic vacuum-filled TO-8 package. The first component of the package is the beryllium window (thickness 100 μm), 1.27 mm behind which is a CdTe crystal (3×3×1 mm) which serves as the active area of the detector. The detector housing, comprised of the head and base of the detector, was also modeled. These included the nickel TO-8 cover, with 14 mm diameter and 0.250 mm thickness, and the 1.5 mm thick base of the TO-8 package, made of Kovar steel (nickel-cobalt ferrous alloy).

3.2 Simplification and Verification of Monte Carlo Model

To speed up computation for subsequent optimization, the first portion of previously described MCNP model was greatly simplified. The section of the model dealing with collimating and filtering the 105 kVp x-ray spectrum from the x-ray source was completely replaced by a new virtual cone-beam source placed directly after the filter. The x-ray energy distribution at this location was determined by experimentally measuring the photon spectrum at that location; this also matched the simulated spectrum at that location fairly well as shown in Fig. 3.2. The new cone-beam source was set to have a divergence that matched the conical collimator, such that the phantom was covered by the beam.

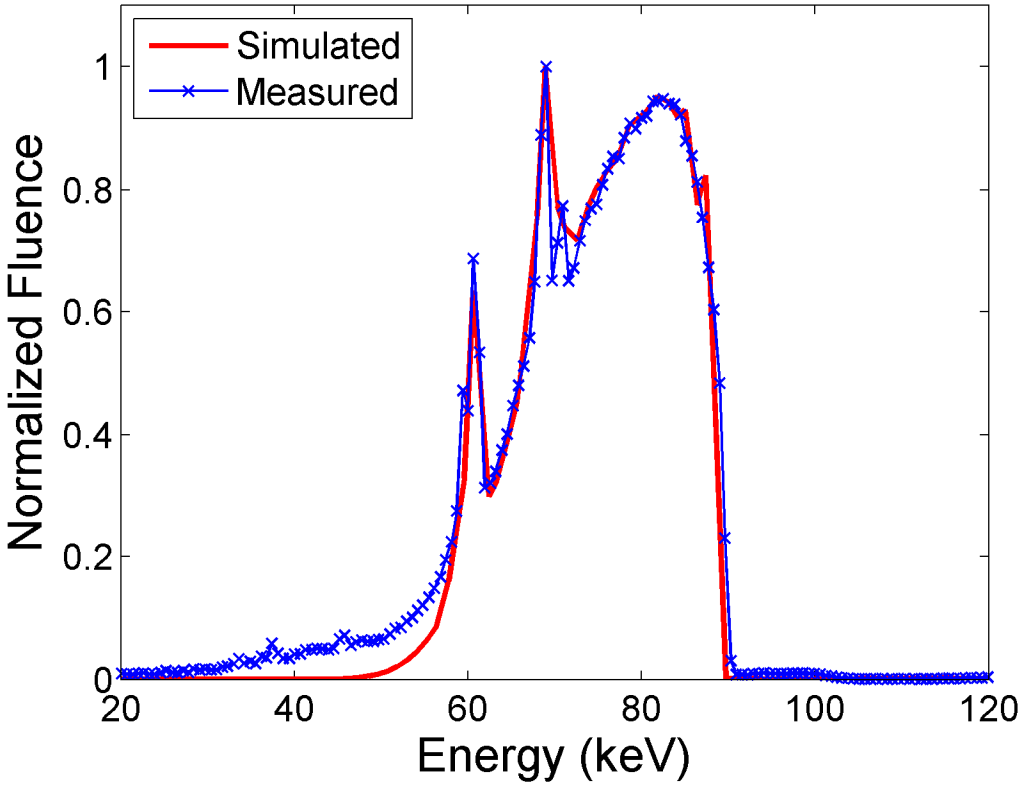

Figure 3.2: Validation of model simplification

By not having to simulate the transport of photons from the actual source through the collimator and filter every time, computational time was shortened dramatically. The beam divergence was kept identical to that of the experimental setup in that the beam just barely covered the diameter of the phantom. Different views of the simplified model are shown in Figs. 3.3, 3.4, and 3.5.

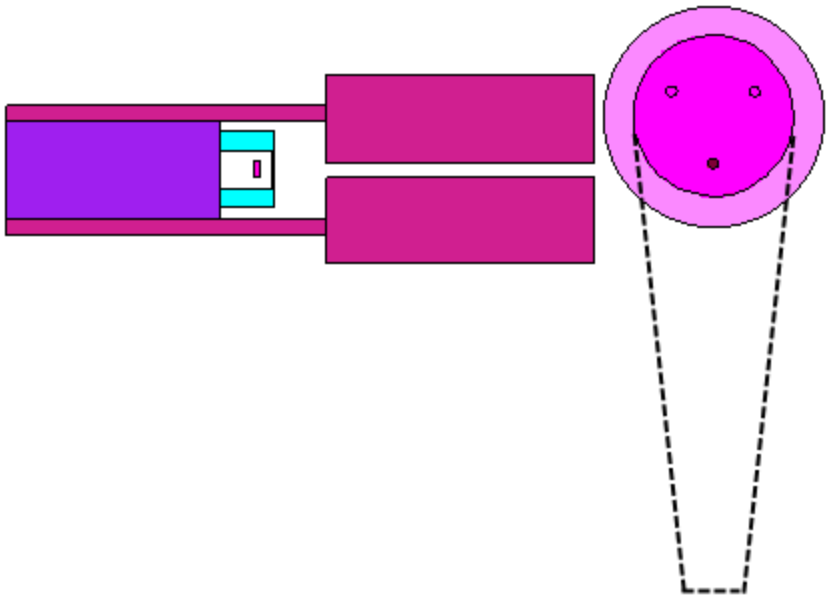

Figure 3.3: Top-down view of simplified MCNP model

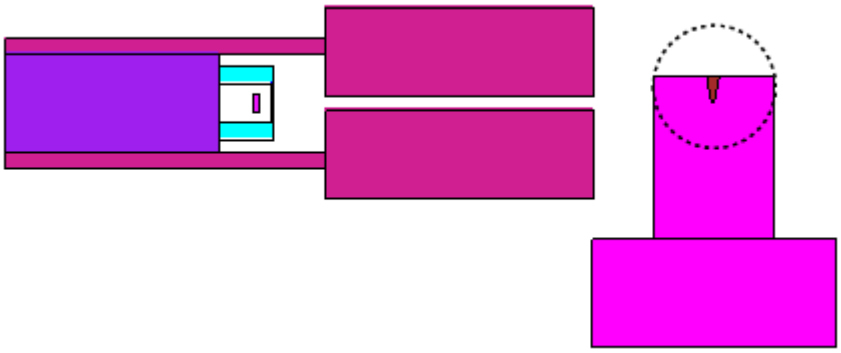

Figure 3.4: Beam's eye view of simplified MCNP model

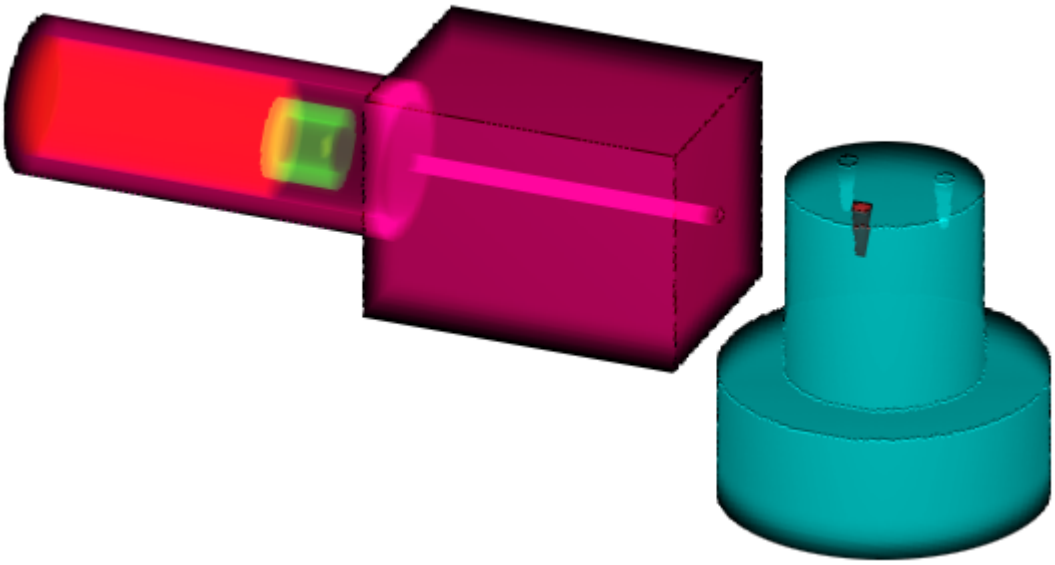

Figure 3.5: Semi-transparent oblique 3D view of simplified MCNP model

The MCNP model was set up to track photons with energy-specific flux (F4) tally done over the CdTe crystal, with the goal of being able to match an experimentally measured x-ray spectrum under the same conditions.

After comparison with experimental results, the preliminary MCNP model with the experimentally-determined source spectrum was verified and found to be an accurate representation of the experimental setup as shown in Fig. 3.6. Since the energy resolution from MC results is inherently very high and is essentially dependent on the bin size, the results were smoothed out such that the full width at half maximum (FWHM) of the gold peaks matched that from the actual measurements; in essence, the energy resolution of the MC results was degraded in order to match the energy resolution of the measurements taken with an actual CdTe detector.

The verification ensured that the model could be used as a tool for further work in order to optimize the experimental setup without actually performing time-consuming and expensive experiments.

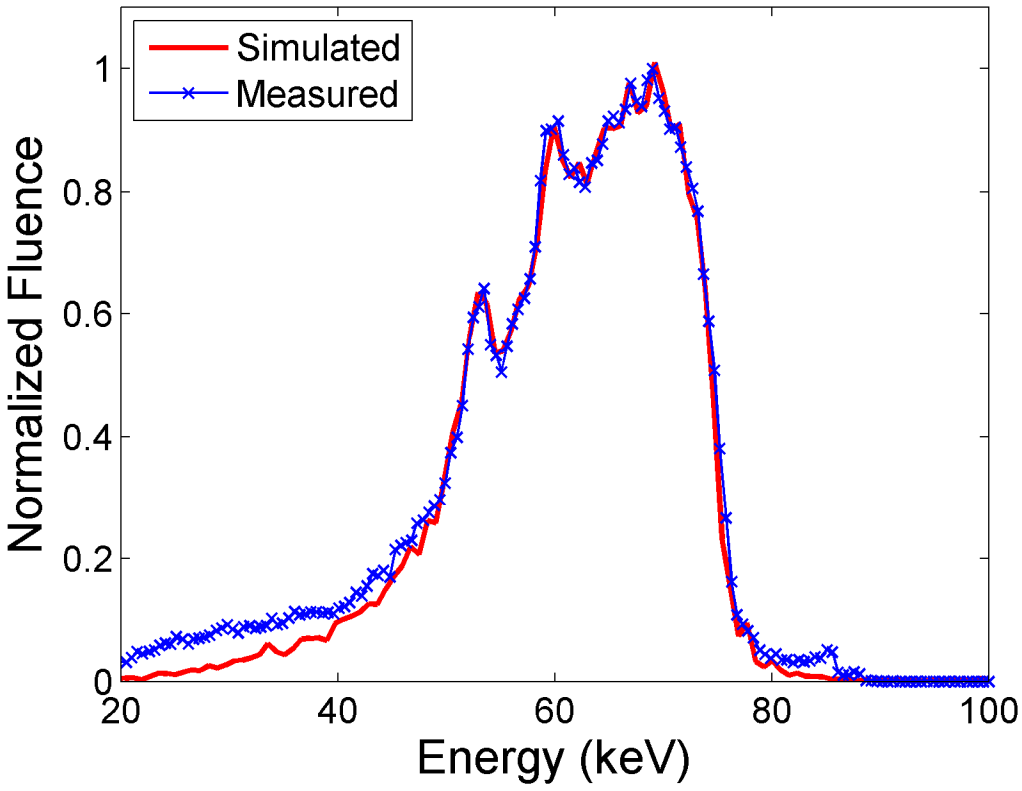

Figure 3.6: Verification of model by comparing simulated and experimental data

3.3 Investigation of Energy Dependence

The energy spectrum of the source was then varied in the MCNP model in order to determine the optimal incident x-ray energy spectrum which would result in the maximum fluorescence production for the given geometry. Due to the physics of the photoelectric interaction, photons of at least 80.7 keV are required to cause *K*-shell fluorescence production from gold. In addition, at the given detector position of 90° with respect to the beam axis, Compton scatter could result in the detection of photons with

energies that obscure the gold fluorescence peaks (67 and 69 keV). To best allow discrimination of the gold peaks, either the Compton scatter peak should appear at comfortably higher energy than the fluorescence peaks or the peaks should be located on a plateau region within the entire spectrum. Noting that the source was operated at 105 kVp, there would be a significant drop-off in x-ray photon fluence as the energy increases up to the maximum of 105 keV. This effectively limited the working range from a minimum of 81 keV to a maximum of 105 keV.

The "hypothetical" source spectra were generated manually. The "simulated" spectrum was generated by using MCNP to simulate the energy-dependent photon fluence after passage of the unaltered x-ray source spectrum through a hypothetical filter material. The measured source spectra were obtained by using the CdTe detector to obtain the energy-dependent photon fluence after passage through filter materials. A correction (Fig. 3.7) was applied to the measured spectra to correct for the energy-dependent efficiency of the CdTe crystal and the Be window[17].

For each simulation set, corresponding to the testing of one spectrum, 80 billion individual particle histories were run in order to obtain statistically significant results. The resulting computational time was on the order of 80 hours for each simulation.

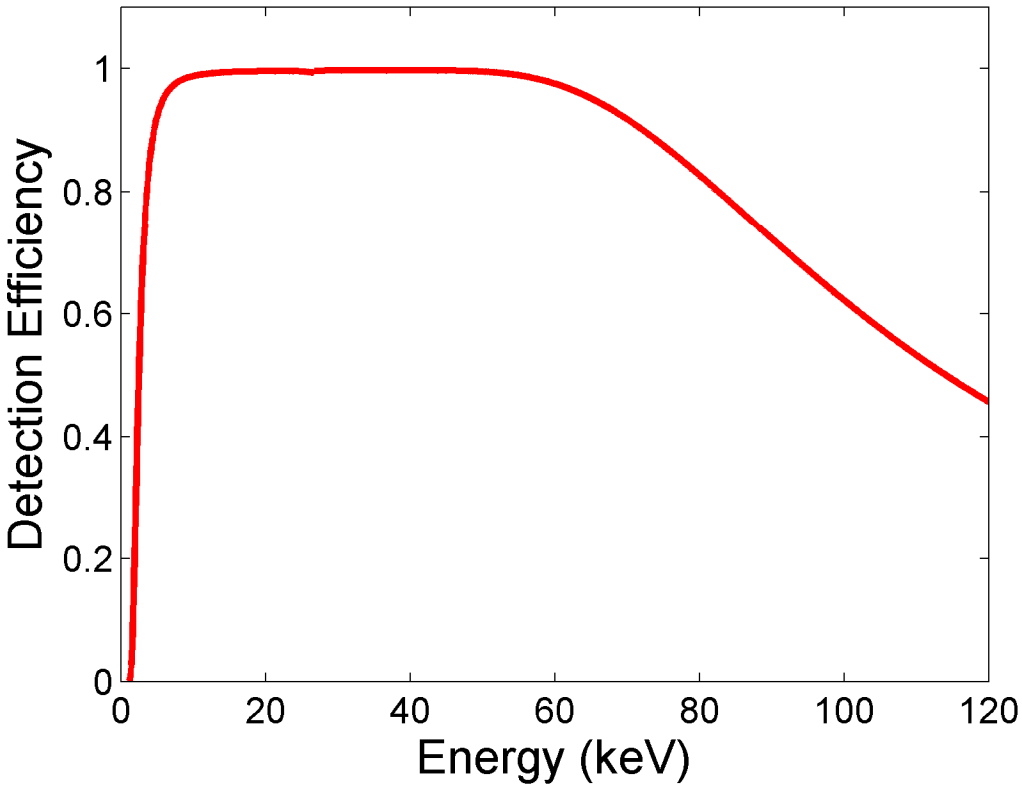

Figure 3.7: Detection efficiency for CdTe-based detector

Table 3.1: Hypothetical, simulated, and measured source spectra

Source Spectrum	Average Energy (keV)	Peak Energy ≥ 81 (keV)
Pb^	72.2	81
Monochromatic*		
81	81	81
85	85	85
90	90	90
95	95	95
100	100	100
Quasi-monochromatic*		
81	81	81
85	85	85
90	90	90
95	95	95
100	100	100
HOPG^	84.7	94
Thoraeus#	84.7	87
Cu + Al^	62.9	81
Sn + Cu^	76.5	84
Sn^	73.1	81

***: hypothetical; #: simulated; ^: measured**

3.3.1 Pb Filtration (Measured)

Since the previous experimental work and initial MC modeling were done with a 1 mm Pb filter as described above, it was used as the benchmark for comparison.

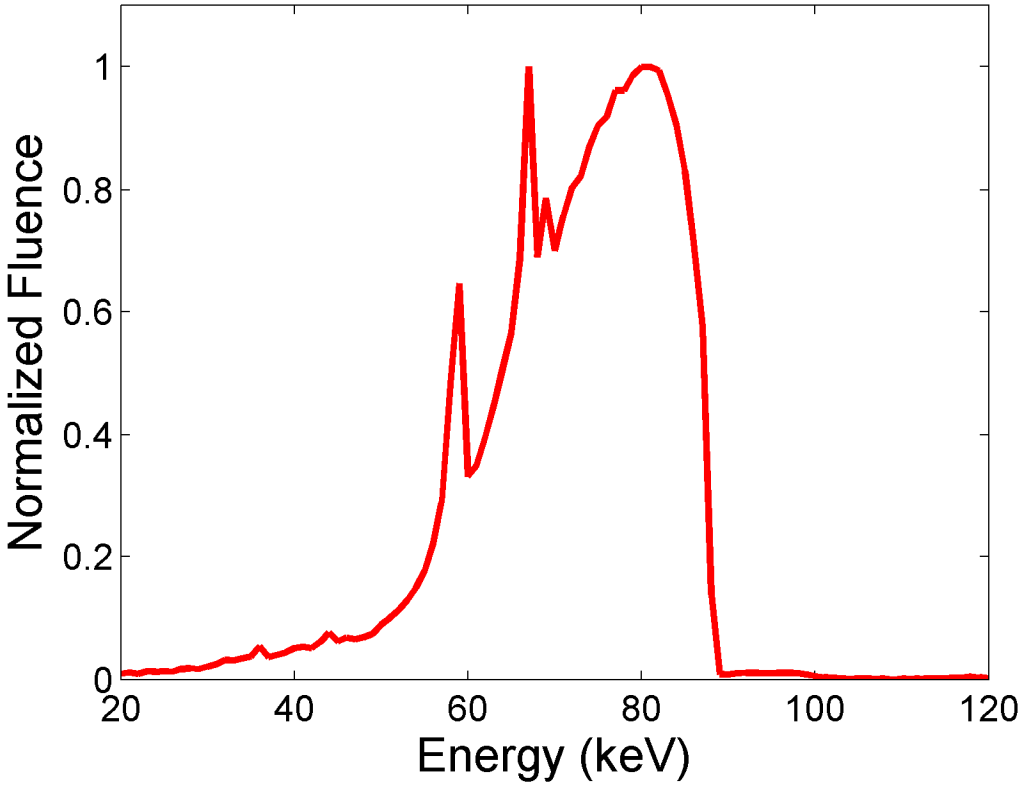

Figure 3.8: Measured spectrum after Pb (1 mm) filtration

3.3.2 Monochromatic Beams (Hypothetical)

Although impossible to produce with an ordinary x-ray tube, monoenergetic source energies of 81, 85, 90, 95, 100 keV were simulated to determine the minimum energy needed to approximately discriminate the gold peaks from the scatter peak. For the scattering angle of 90°, the respective scattered photon energies for 81, 85, 90, 95, and 100 keV source photons would be 70, 73, 77, 80, and 84 keV. Higher energies would theoretically be better since the scattered peak would not overshadow the gold fluorescence peaks. However, at these energies, the polychromatic 105 kVp x-ray spectrum had atrociously low fluence; although beyond the scope of this work, this limitation was kept in mind.

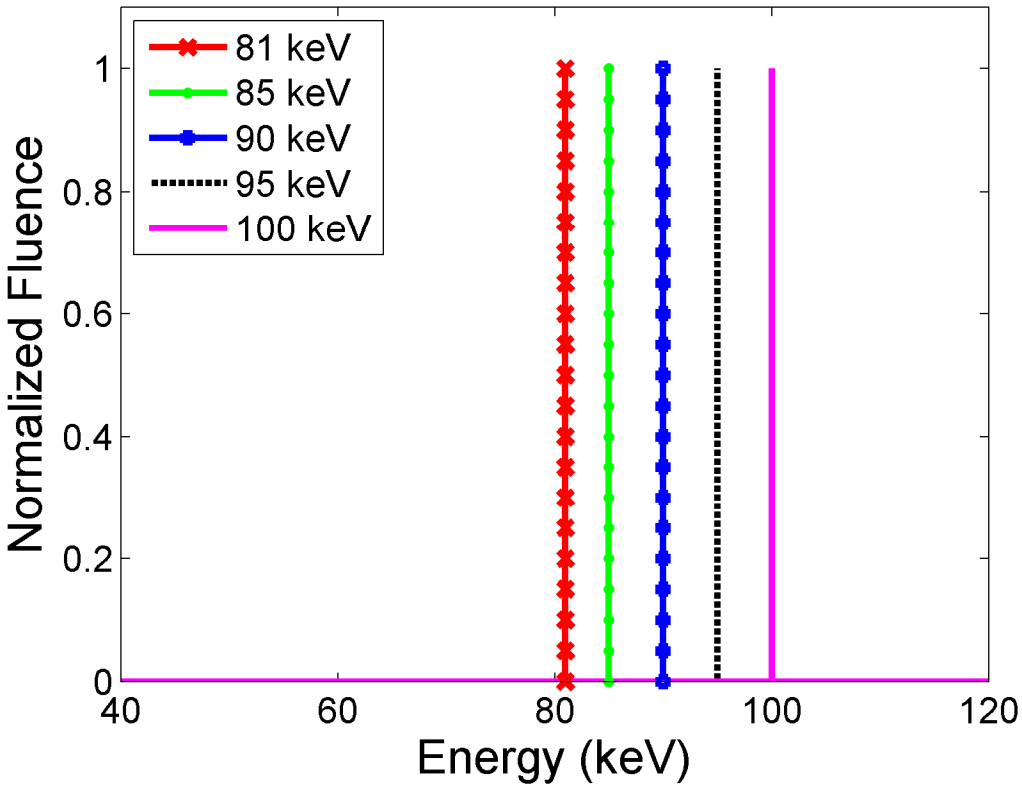

Figure 3.9: Hypothetical monochromatic beam spectra

3.3.3 Quasi-monochromatic Beams (Hypothetical)

Noting that even a synchrotron cannot produce perfectly monochromatic beams, the slightly more practical case of quasi-monochromatic beams peaking at 81, 85, 90, 95, and 100 keV with Gaussian FWHM of 10 keV were generated and used for simulations.

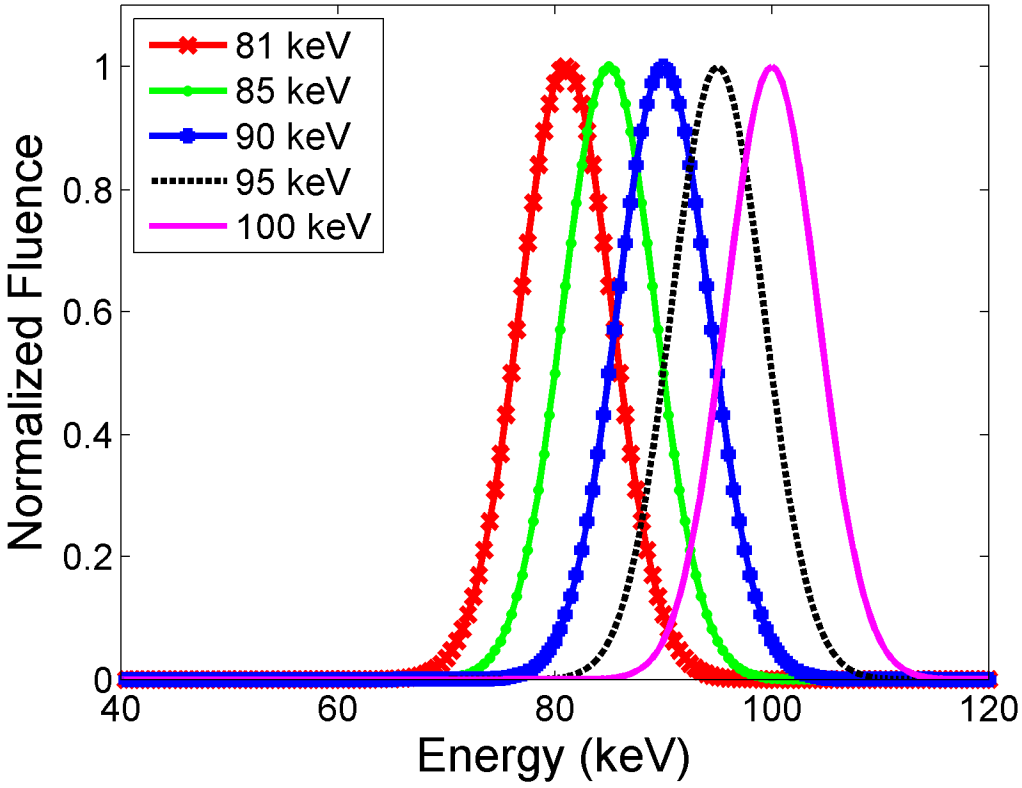

Figure 3.10: Hypothetical quasi-monochromatic beam spectra

3.3.4 HOPG Monochromatization (Measured)

Once the optimal energy (95 keV) was determined from the quasi-monochromatic beam simulations, the 105 kVp x-ray tube output was reflected off of a highly ordered pyrolytic graphite (HOPG) crystal in a specific manner to produce an actual spectrum that peaked at approximately 95 keV [18]. This spectrum was measured by a CdTe detector [7] and used for simulations.

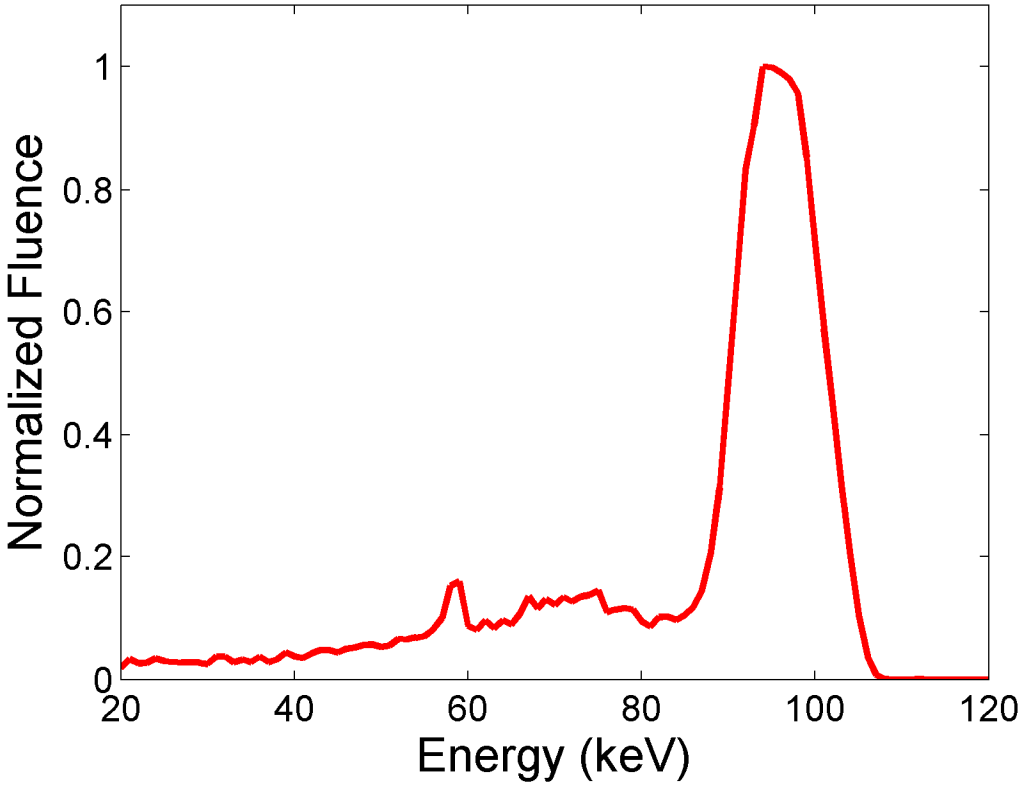

Figure 3.11: Measured spectrum after HOPG reflectance

3.3.5 Thoraeus Filtration (Simulated)

Since using HOPG was quite cumbersome, conventional filters were considered. MCNP was employed to simulate filtration of the 105 kVp source spectrum through a Thoraeus-type filter (2 mm Sn, 0.5 mm Cu, 4 mm Al) [19]. The resulting spectrum was noisy and the statistics below 60 keV were very poor so only the data between 60 keV and 100 keV were used, which was considered to be acceptable for the purpose of exploratory simulations. The spectrum peaked at around 90 keV.

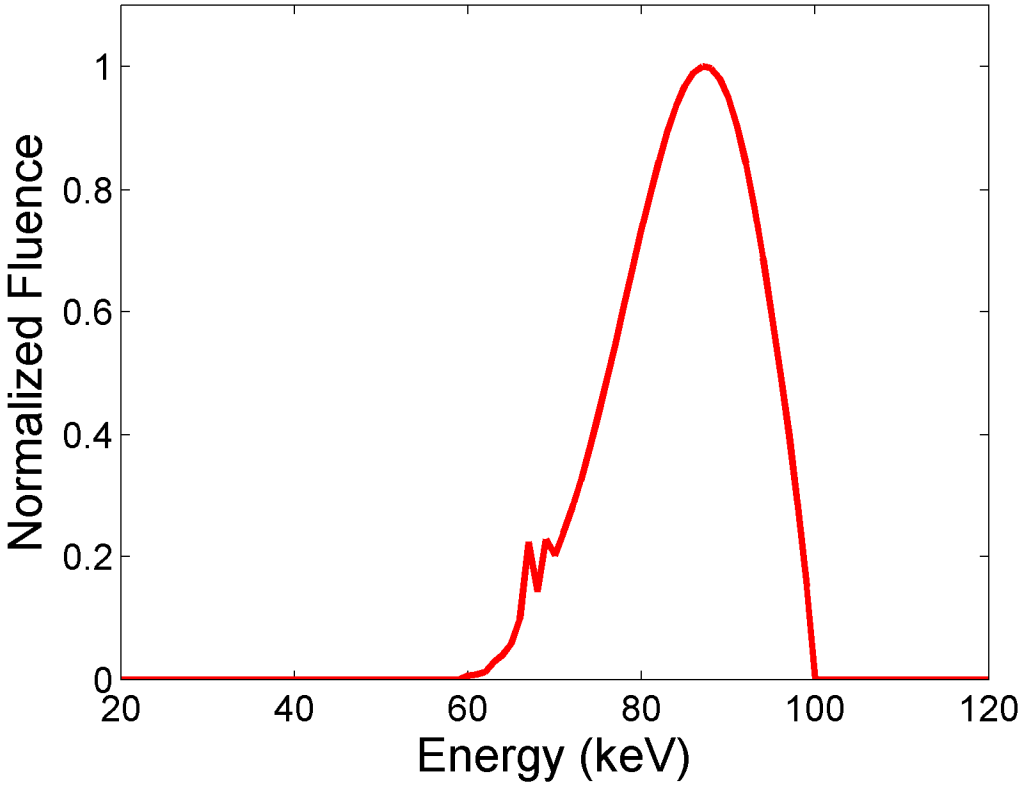

Figure 3.12: Simulated spectrum after Thoraeus filtration

3.3.6 Sn and Cu Filtration (Experimental)

Inspired by simulations with the Thoraeus-type filter, experimental work was done to obtain a spectrum resulting from filtering the 105 kVp beam through Sn (0.8 mm) and Cu (0.65 mm). Al was omitted with the intent of preserving some fluence; however, this was limited to lower energy photons which would not contribute to fluorescence production anyway.

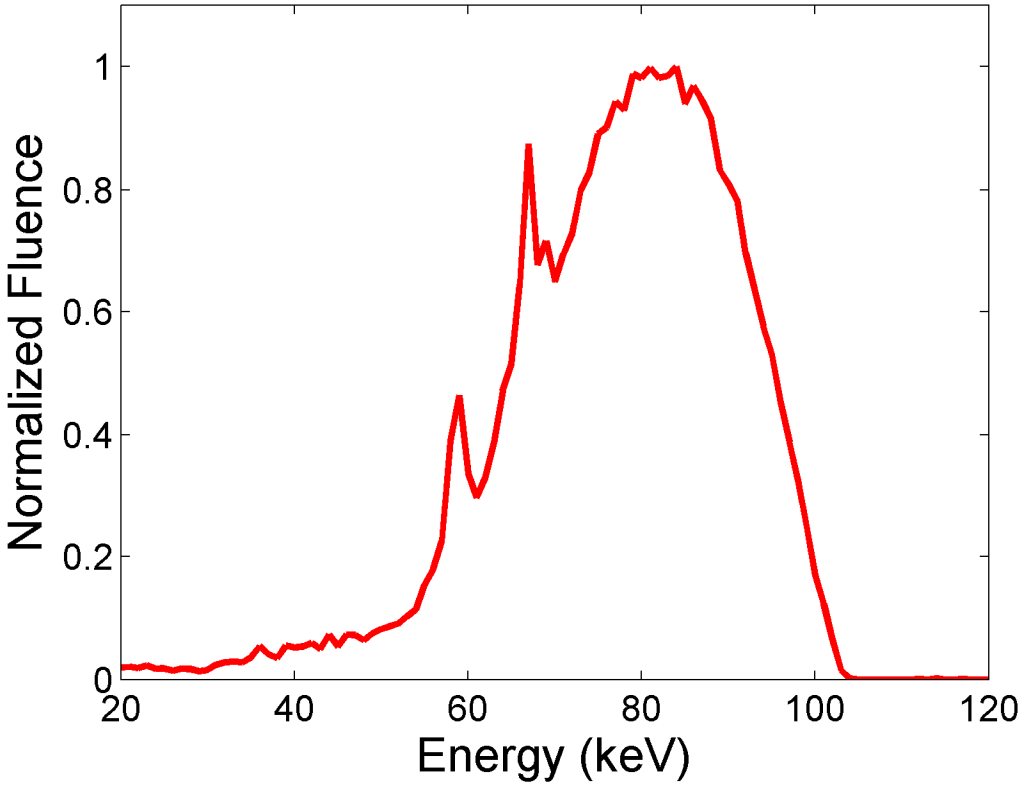

Figure 3.13: Measured spectrum after Sn (0.8 mm) and Cu (0.65 mm) filtration

3.3.7 Cu and Al Filtration (Measured)

Another experiment with filtration using Cu (3.6 mm) and Al (2 mm) yielded a spectrum with more overall fluence than the previously described Sn and Cu filter. Although Sn was omitted, the increased thickness of Cu suppressed many of the higher energy photons.

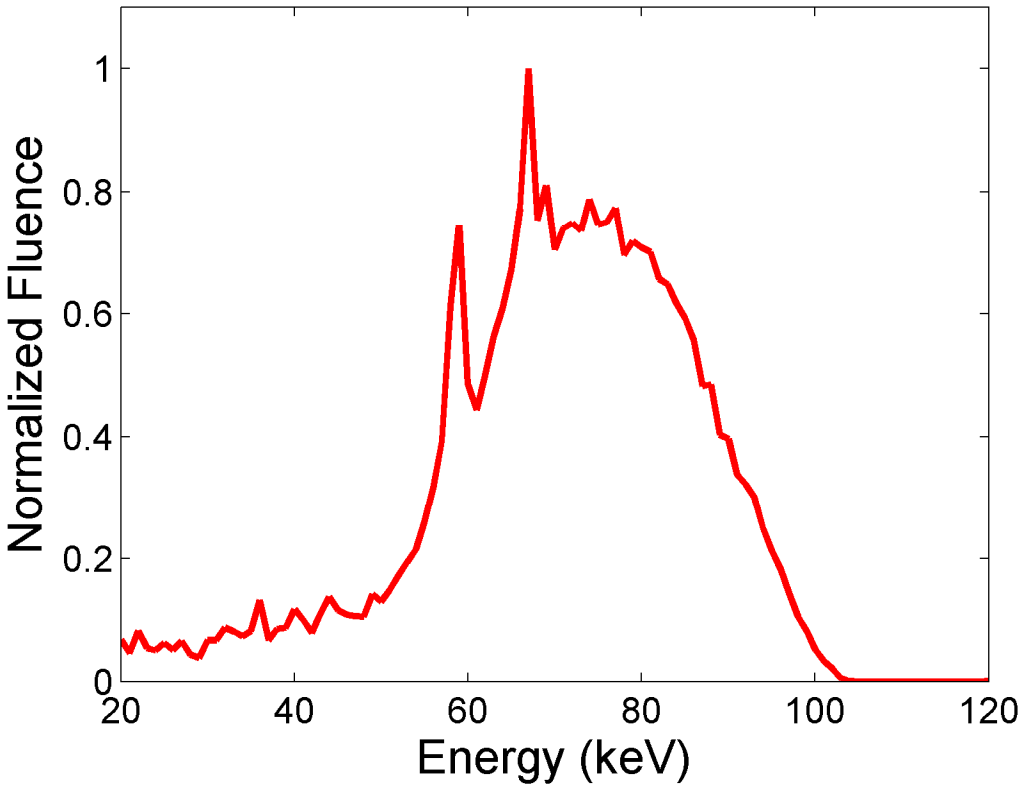

Figure 3.14: Measured spectrum after Cu (3.6 mm) and Al (2 mm) filtration

3.3.8 Sn Filtration (Experimental)

Finally, it was decided that Cu can be omitted to increase overall fluence while maintaining the beam hardening properties of Sn. A Sn filter of 0.8 mm was used to filter the 105 kVp beam.

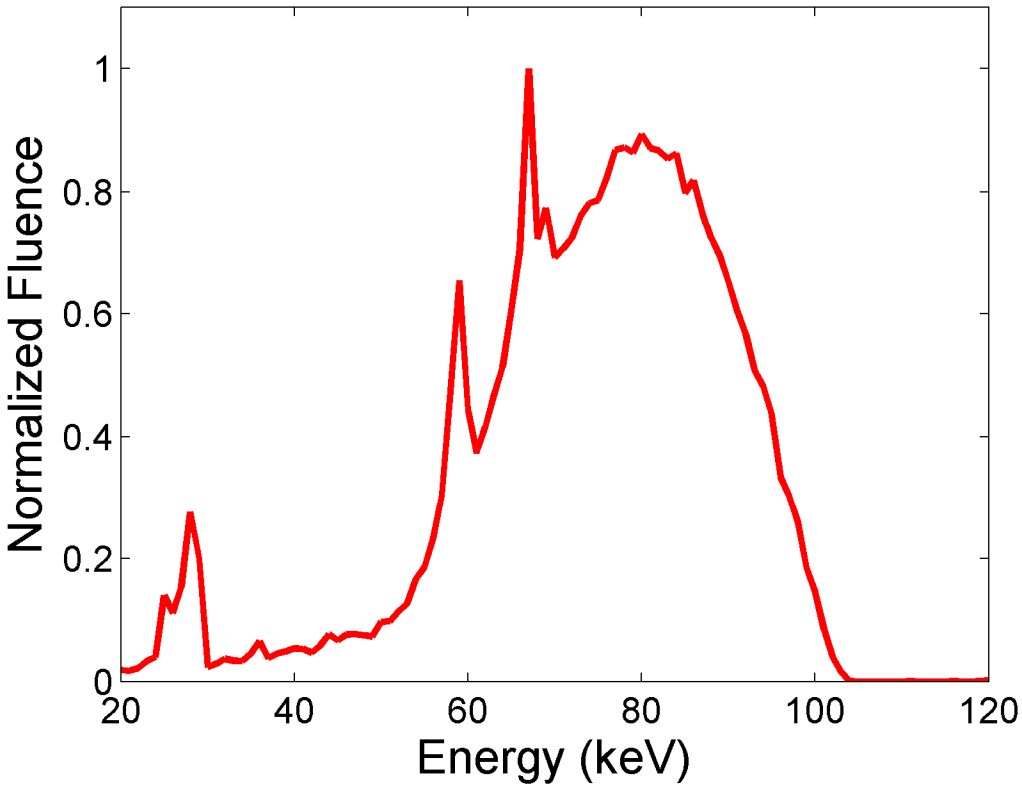

Figure 3.15: Measured spectrum after Sn (0.8 mm) filtration

CHAPTER 4

RESULTS

The overall scatter profile from each simulation was obtained from 20 to 100 keV. The gold peaks of interest are the *K*-shell alpha peaks at 67 and 69 keV. The less prominent *K*-beta peak at around 78 keV was visible in some of the results but it was not considered for analysis. Since smoothing was not applied, the energy resolution was on the order of the bin size (approximately 0.5 keV). With the 80 billion histories simulated for each case, the average statistical uncertainty over the entire tally was on the order of 0.5%.

4.1 Scatter Profile Spectra

4.1.1 Pb Filtration

These results using the Pb filtered source have been shown previously, albeit with smoothing. The region around the gold peaks, although relatively flat, had the highest fluence of the entire scatter profile. In other words, the gold peaks were superposed on the primary Compton scatter peak which was located in the same 67-69 keV region of interest.

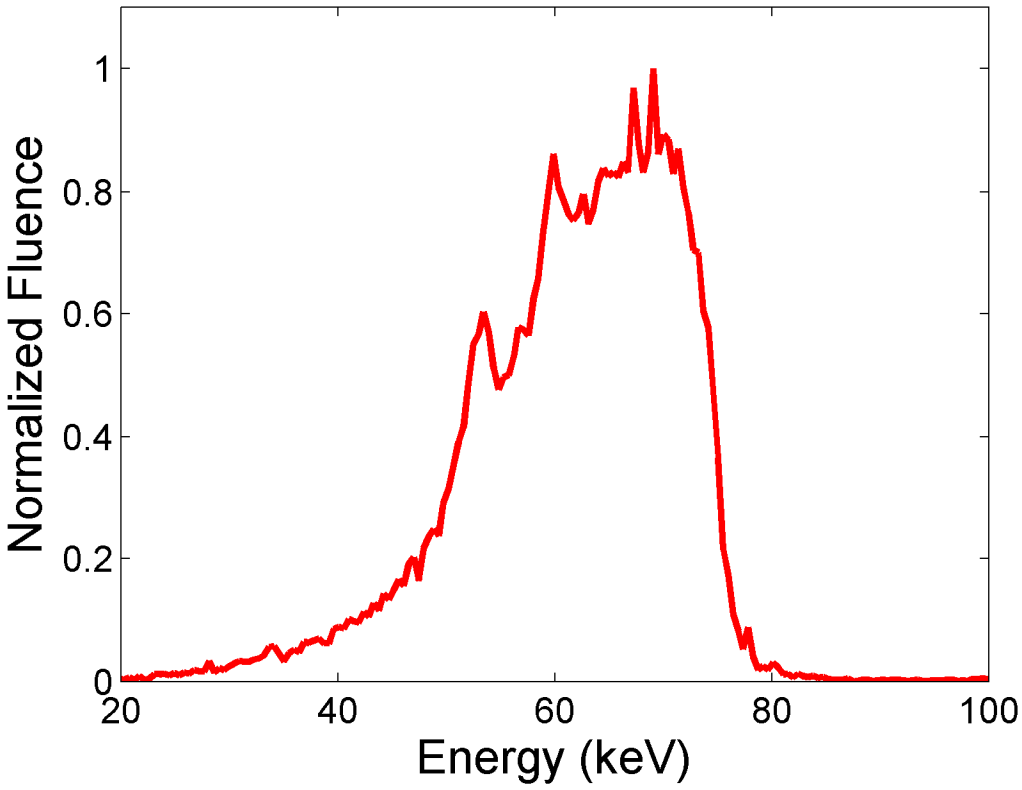

Figure 4.1: Scatter profile for Pb filtered source spectrum

4.1.2 Monochromatic Beams (Simulated)

The results from using the monochromatic source spectra were very insightful. A few observations were immediately evident. As the source energy was increased, the Compton scatter peak shifted to higher energies, as expected. When the source energy was 81 keV, the gold peaks were almost completely obscured by the Compton scatter peak which occurred at around 70 keV. At higher source energies, the gold peaks were more discernible.

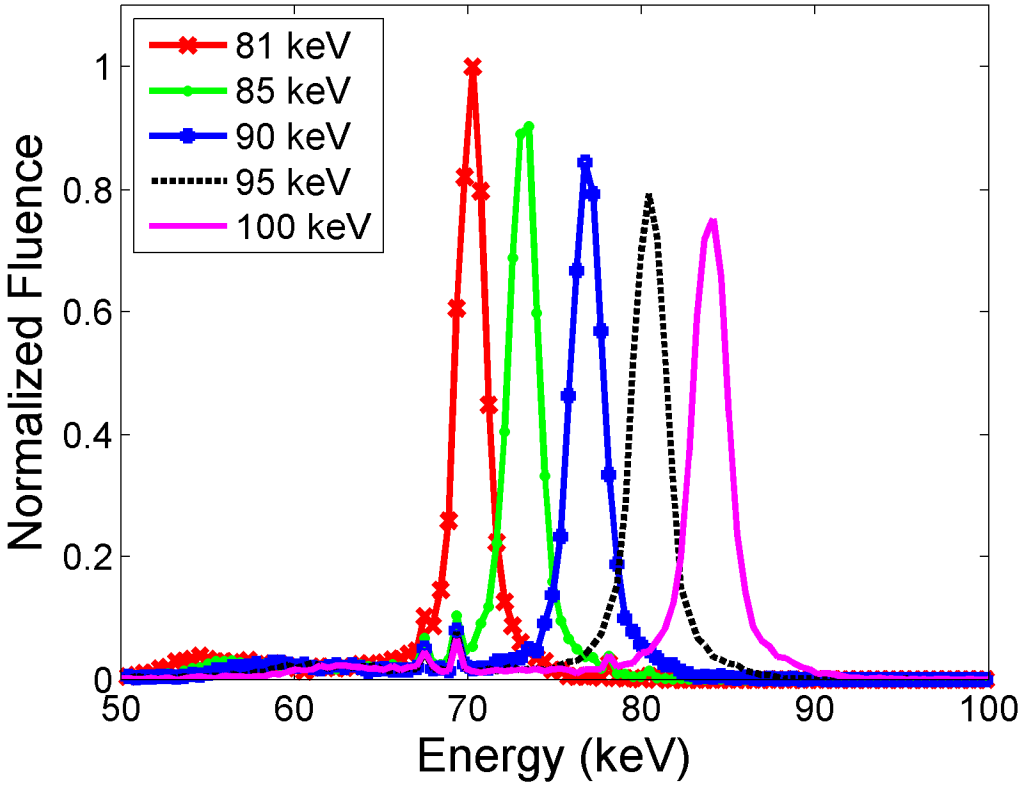

Figure 4.2: Scatter profile for monochromatic source spectra

4.1.3 Quasi-monochromatic Beams (Simulated)

The quasi-monochromatic source spectra resulted in similar scatter profiles as the monochromatic source spectra but with some slight differences. Qualitatively speaking, the energy needed to be at least 95 keV for the gold peaks to be fully discernible from the scatter peak. At lower energies, the peaks appeared on the shoulder of the scatter peak, making it difficult to discern them from the inherent features of the scatter background itself.

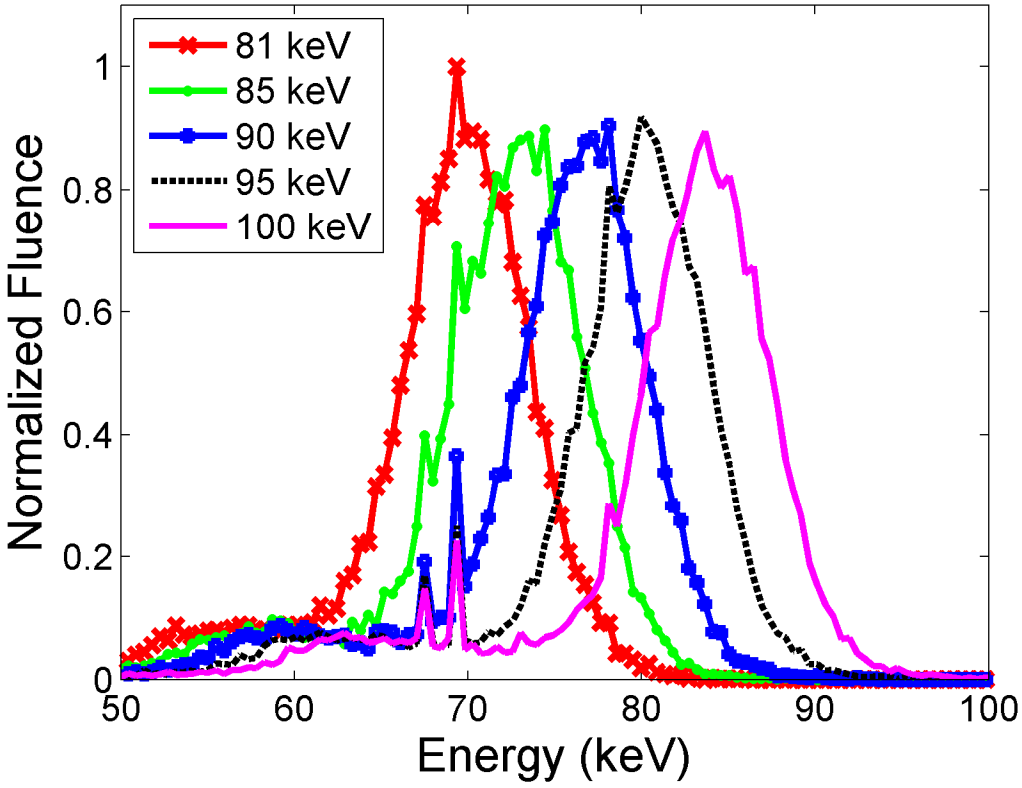

Figure 4.3: Scatter profile for quasi-monochromatic source spectra

4.1.4 HOPG Monochromatization

The scatter profile for the HOPG spectrum looked strikingly similar to the 95 keV quasi-monochromatic results. This was expected since both spectra peaked around 95 keV, although the HOPG spectrum had a higher fluence of lower energy photons which would not contribute to *K*-shell fluorescence from gold anyway.

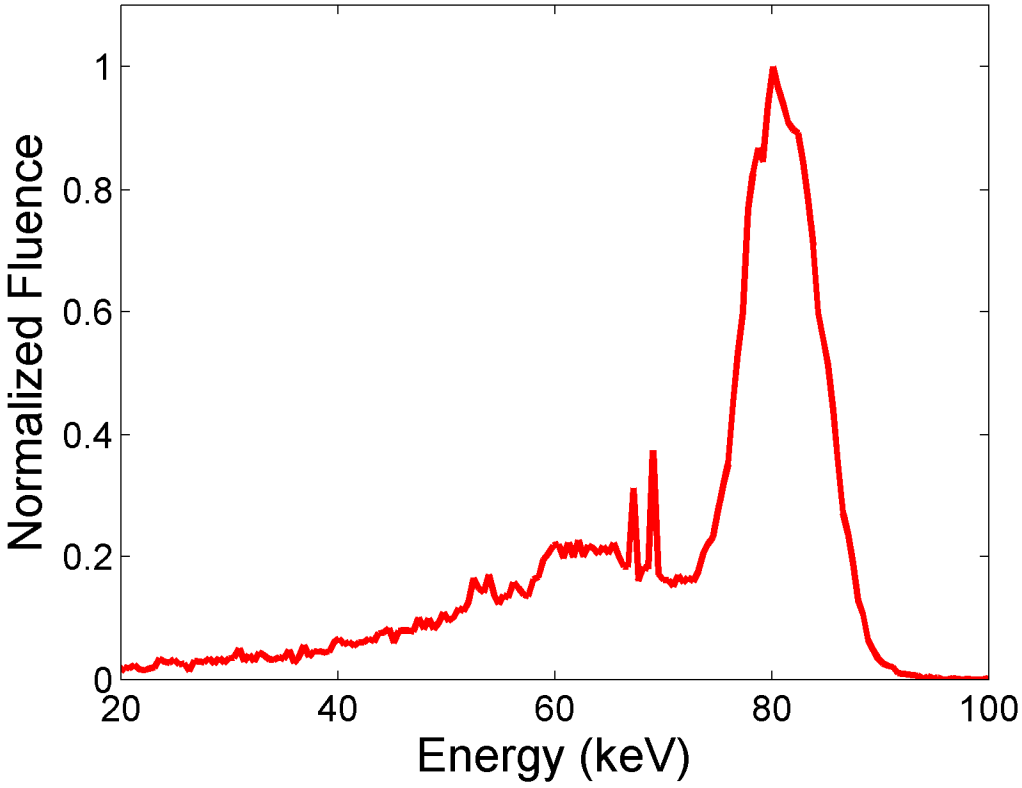

Figure 4.4: Scatter profile for HOPG-monochromatized source spectrum

4.1.5 Thoraeus Filtration

The results from using the Thoraeus-type filter looked like a combination of the 85 and 90 keV quasi-monochromatic beam results. The gold peaks appeared on the shoulder of the scatter peak but they were quite prominent.

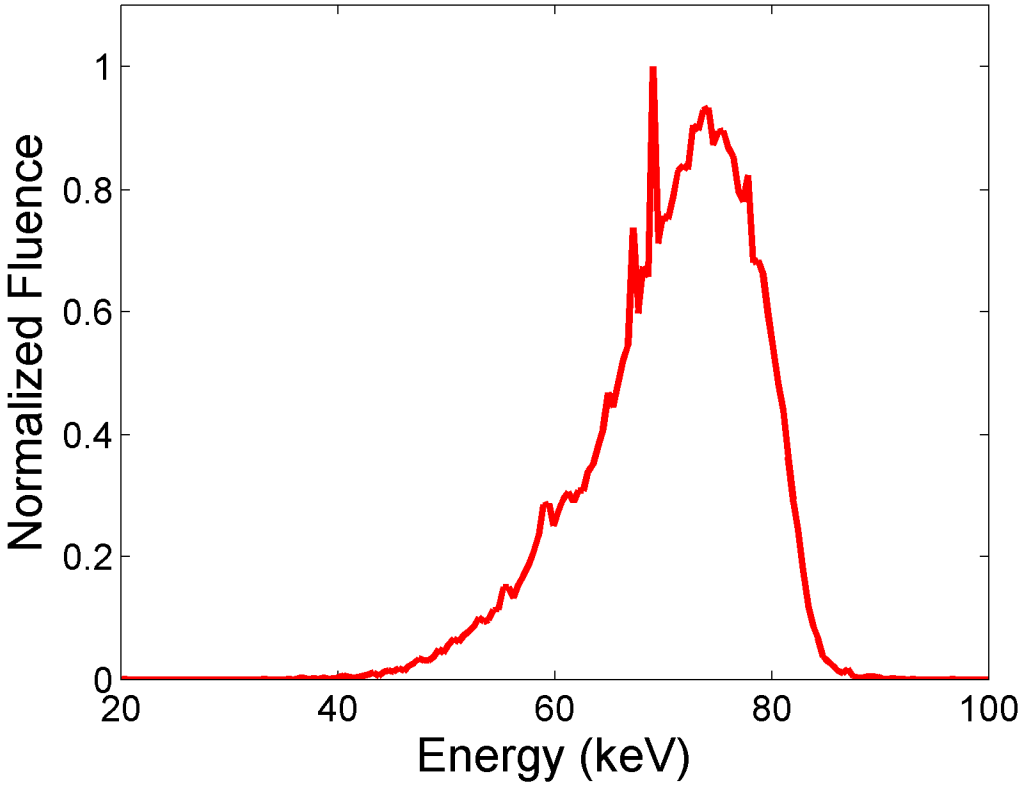

Figure 4.5: Scatter profile for Thoraeus filtered source spectrum

4.1.6 Sn and Cu Filtration

Using Sn and Cu for filtration decreased much of the lower energy photons while preserving the higher energies. Also, the scatter peak became very spread out and thus, the gold peaks were located on a plateau region, making them easy to discern.

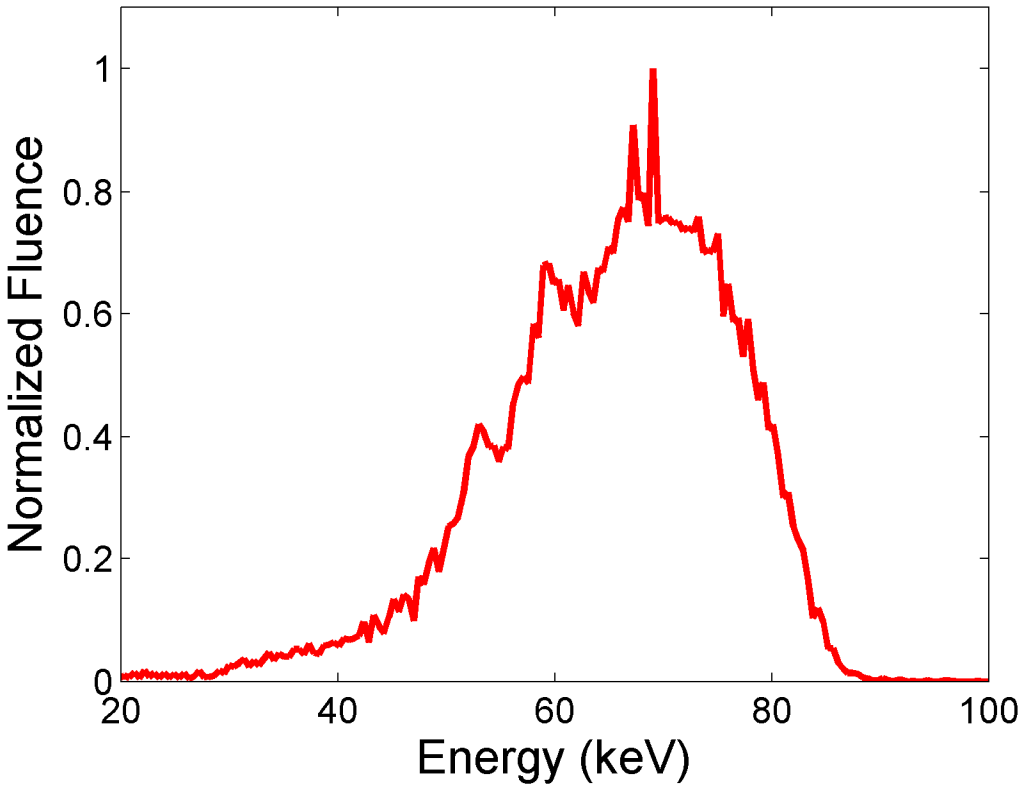

Figure 4.6: Scatter profile for Sn and Cu filtered source spectrum

4.1.7 Cu and Al Filtration

Removal of the Sn and addition of Al and a thicker Cu filter produced some interesting effects. Relatively speaking, lower energy fluence increased. The characteristic peaks from the source showed up prominently, overshadowing the gold peaks which occurred on the right shoulder of the scatter profile.

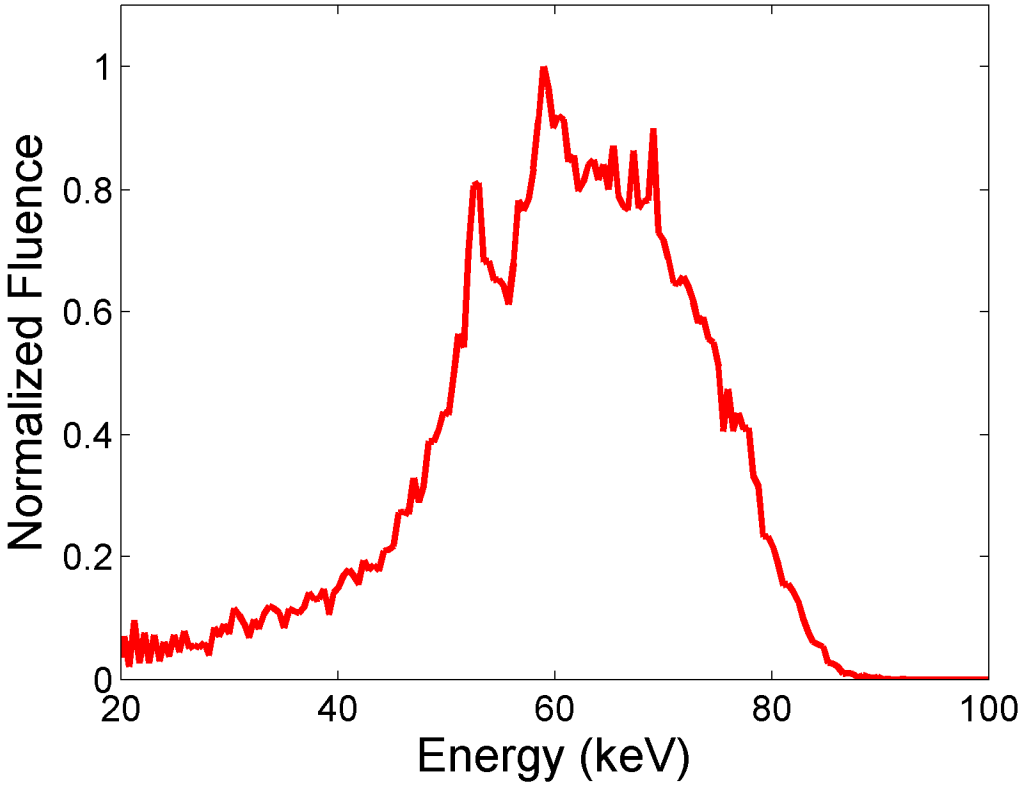

Figure 4.7: Scatter profile for Cu and Al filtered source spectrum

4.1.8 Sn Filtration

Using only a Sn filter resulted in a scatter profile similar to that obtained from using Sn and Cu albeit with more relative fluence at lower energies. The gold peaks appeared on a plateau region once again.

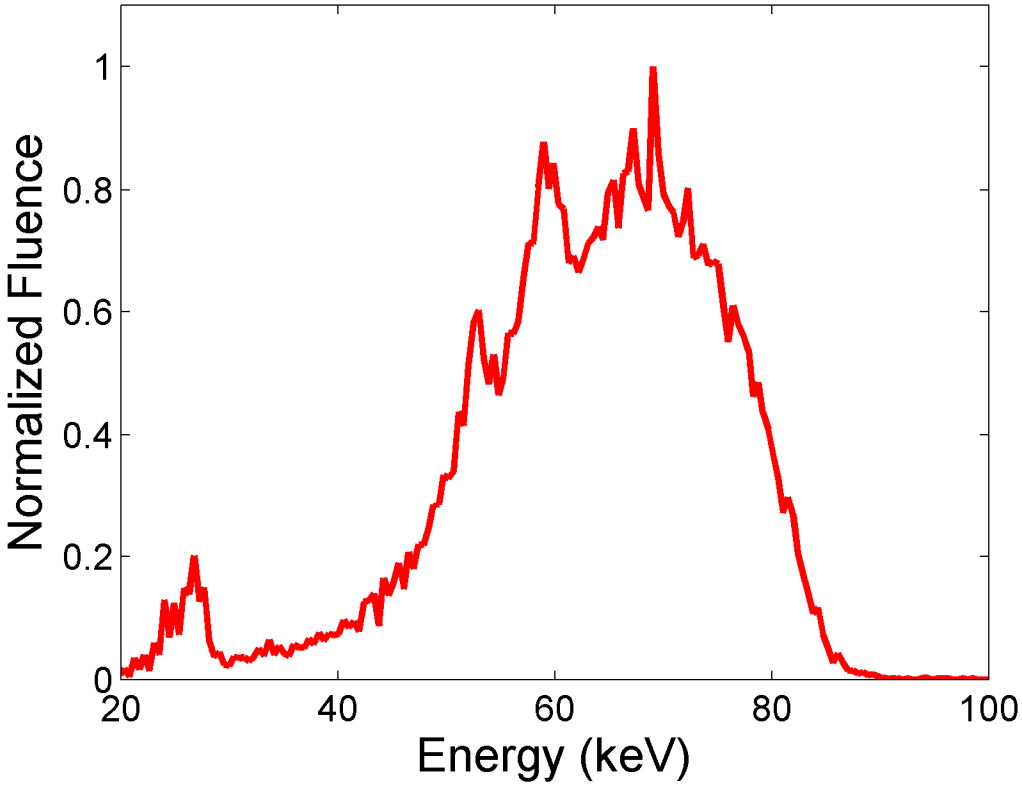

Figure 4.8: Scatter profile for Sn filtered source spectrum

4.2 Signal-to-Background Ratio and "Flatness" Calculations

For a more quantitative measure of judging the effect of the source spectrum on gold fluorescence production, the signal-to-background ratio (SBR) was used. Calling the bins where the 67 and 69 keV peaks occur "i" and "j" respectively, the SBR was calculated using linear interpolation between the neighboring bins.

$$SBR_i = \frac{A_i}{\frac{1}{2}(A_{i-1} + A_{i+1})}; \; SBR_j = \frac{A_j}{\frac{1}{2}(A_{j-1} + A_{j+1})}$$

Also, the "flatness" (F) was calculated as the reciprocal of the slope using the following relation.

$$F = \frac{E_{j+1} - E_{i-1}}{A_{j+1} - A_{i-1}}$$

In both cases, a larger value represents a better outcome. A side effect of the fine bin size was that the SBR for the simulated results was much higher than that which was seen in experimental results. However, for the purpose of this work, this was not a concern as consistency was maintained and the large SBR was actually preferable for illustrative purposes.

Table 4.1: Signal-to-background ratio and "flatness" data

	Peak-Specific			
Source Spectrum	**67 keV**	**69 keV**	**Average**	**"Flatness"**
Pb^	1.13	1.16	1.15	94.2
Monochromatic*				
81	1.53	1.12	1.33	3.6
85	2.59	2.58	2.59	120.9
90	2.80	4.18	3.49	569.7
95	2.71	5.10	3.91	1346400.0
100	2.07	4.14	3.11	939.1
Quasi-monochromatic*				
81	1.15	1.15	1.15	9.7
85	1.39	1.34	1.36	7.8
90	2.27	2.89	2.58	35.3
95	2.91	4.17	3.54	452.7
100	2.44	3.91	3.17	148.2
HOPG^	1.82	2.13	1.98	233.0
Thoraeus#	1.29	1.46	1.37	16.7
Cu + Al^	1.12	1.19	1.16	71.3
Sn + Cu^	1.18	1.34	1.26	1485.3
Sn^	1.10	1.23	1.16	96.4

***: hypothetical; #: simulated; ^: measured**

4.3 Summary of Findings

Based on the obtained scatter profiles and from the signal-to-background ratio calculations, it was immediately obvious that the source spectrum has a major effect on the production and detectability of fluorescence from the GNPs.

The experimentally-used 1 mm Pb filter resulted in a simulated signal-to-background ratio (SBR) of about 115% for the gold fluorescence peaks. The hypothetical monochromatic and quasi-monochromatic spectra showed that monochromatization could result in dramatic improvements. For example, using a hypothetical 95 keV monochromatic beam could result in a SBR of 391%, a 3.4-fold increase over the Pb filtration. Furthermore, the "flatness" of the 67-69 keV region was extremely high, which would facilitate differentiation of the gold peaks from the background.

Using HOPG monochromatization to produce a potentially realistically obtainable spectrum, the SBR was around 198%, a 1.7-fold increase over the Pb filtered source. A more conventional filtration method using a Thoraeus-type filter resulted in a SBR of 137%, a 1.19-fold increase. Various combinations of filtration materials also showed some improvement over the Pb filtration. Of note, the Sn and Cu filtration resulted in a SBR of 126% and a remarkably high "flatness" value for the region of interest.

CHAPTER 5

CONCLUSION AND FUTURE WORK

In this work, an experimental XFCT system was modeled using the MCNP code system. After validation of the MCNP model as an accurate representation of the experimental setup, it was used for further simulations to study the effects of source energy spectra on the detection of fluorescence photons from GNPs. It was found that monochromatization, using atypical methods as well as conventional filtration, significantly improved the signal-to-background ratio of the gold peaks.

It is important to note that this study focused on the effects of source spectra only, without much consideration for the effects of filtration on absolute fluence. Lowering the absolute fluence would result in longer scanning time and perhaps. Ideally, the fluence below 81 keV would be fully eliminated. A very exhaustive and methodological study needs to be done with varying filter thicknesses to find the optimal values. Furthermore, the simulated results need to be verified with experiments.

Considering that every hypothetical and experimental filter utilized in this work resulted in improvements over the 1 mm Pb filter used for the previous experimental work, this work has set the stage for further optimization of the experimental XFCT system. This work will foster the further development of the XFCT system in the context of making it more practical for GNP-based preclinical molecular imaging applications.

REFERENCES

[1] D. B. Chithrani, et al., *Gold nanoparticles as radiation sensitizers in cancer therapy.* Radiation Research, 2010. **173**(6): p. 719-728.

[2] S. H. Cho, *Estimation of tumour dose enhancement due to gold nanoparticles during typical radiation treatments: a preliminary Monte Carlo study.* Physics in Medicine and Biology, 2005. **50**(15): p. N163-73.

[3] J. F. Hainfeld, et al., *Gold nanoparticles: a new X-ray contrast agent.* British Journal of Radiology, 2006. **79**(939): p. 248.

[4] S. H. Cho, B. L. Jones, and S. Krishnan, *The dosimetric feasibility of gold nanoparticle-aided radiation therapy (GNRT) via brachytherapy using low-energy gamma-/x-ray sources.* Physics in Medicine and Biology, 2009. **54**(16): p. 4889-905.

[5] J. F. Hainfeld, et al., *Radiotherapy enhancement with gold nanoparticles.* Journal of Pharmacy and Pharmacology, 2008. **60**(8): p. 977-85.

[6] B. L. Jones, *Monte Carlo calculations of microscopic dose enhancement for gold nanoparticle-aided radiation therapy*. MS Thesis, 2009. Georgia Institute of Technology.

[7] B. L. Jones, *Development of dosimetry and imaging techniques for pre-clinical studies of gold nanoparticle-aided radiation therapy*. PhD Dissertation, 2011. Georgia Institute of Technology.

[8] B. L. Jones, S. Krishnan, and S. H. Cho, *Estimation of microscopic dose enhancement factor around gold nanoparticles by Monte Carlo calculations.* Medical Physics, 2010. **37**(7): p. 3809-16.

[9] S-K. Cheong, et al., *X-ray fluorescence computed tomography (XFCT) imaging of gold nanoparticle-loaded objects using 110 kVp x-rays.* Physics in Medicine and Biology, 2010. **55**(3): p. 647-62.

[10] B. L. Jones and S. H. Cho, *The feasibility of polychromatic cone-beam x-ray fluorescence computed tomography (XFCT) imaging of gold nanoparticle-loaded objects: a Monte Carlo study.* Physics in Medicine and Biology, 2011. **56**(12): p. 3719.

[11] G. F. Rust and J. Weigelt, *X-ray fluorescent computer tomography with synchrotron radiation.* IEEE Transactions on Nuclear Science, 2005. **45**(1): p. 75-88.

[12] G. Jost, et al., *Imaging-therapy computed tomography with quasi-monochromatic x-rays.* European Journal of Radiology, 2008. **68**(3): p. S63-S68.

[13] G. Jost, et al., *Photoelectric-enhanced radiation therapy with quasi-monochromatic computed tomography.* Medical Physics, 2009. **36**: p. 2107.

[14] F. Liu, *Monte Carlo modeling of an x-ray fluorescence detection system by the MCNP code*. MS Thesis, 2009. Georgia Institute of Technology.

[15] X-5 Monte Carlo Team, *MCNP - A General Purpose Monte Carlo N-Particle Transport Code, Version 5*. LA-UR-03-1987, 2003.

[16] Amptek Inc., *X-Ray and Gamma Ray Detector: XR-100T-CdTe*. Available from: http://www.amptek.com/xr100cdt.html. Accessed: Dec. 2009

[17] M. J. Berger, et al., *XCOM: Photon Cross Section Database*. 2010; Available from: http://physics.nist.gov/xcom. Accessed: Dec. 2010

[18] I. G. Grigorieva and A. A. Antonov, *HOPG as powerful x-ray optics.* X-Ray Spectrometry, 2003. **32**(1): p. 64-68.

[19] F. H. Attix, *Introduction to Radiological Physics and Radiation Dosimetry*. 1986: Wiley-VCH.